www.czasopisma.pan.pl PAN POLSKA AKADEMIA NAUK www.journals.pan.pl

Arch. Metall. Mater. **67** (2022), 4, 1525-1529

DOI: https://doi.org/10.24425/amm.2022.141087

SO-YEON PARK[1], KYU-SIK KIM[2], BANDAR ALMANGOUR[3], KEE-AHN LEE[1*]

EFFECT OF MICROSTRUCTURE AND UNIT CELL'S GEOMETRY ON THE COMPRESSIVE MECHANICAL RESPONSE OF ADDITIVELY MANUFACTURED Co-Cr-Mo SHEET I-WP LATTICE

Co-Cr-Mo based sheet I-WP lattice was fabricated via laser powder bed fusion. The effect of microstructure and the I-WP shape on compressive mechanical response was investigated. Results of compression test showed that yield strength of the sheet I-WP was 176.3 MPa and that of bulk Co-Cr-Mo (reference material) was 810.4 MPa. By applying Gibson-Ashby analytical model, the yield strength of the lattice was reversely estimated from that of the bulk specimen. The calculated strength of the lattice obtained was 150.7 MPa. The shape of deformed lattice showed collective failure mode, and its microstructure showed that strain-induced martensitic transformation occurred in the overall lattice. The deformation behavior of additively manufactured sheet I-WP lattice was also discussed.

Keywords: Laser powder bed fusion; Co-Cr-Mo; sheet I-WP lattice; Compressive mechanical response; Strain-induced martensitic transformation

1. Introduction

A lattice structure is defined as an architecture having regularly repeated unit cells, and is applied in a wide range of fields using the unit cell's structural characteristics and intrinsic properties of the parent material [1-6]. Recent advances in additive manufacturing (AM) technology have led to an accelerated growth in the field of lattice structure. This is because applying the AM technology in the syntheses of lattice removes the restrictions on material selection and allows designing and manufacturing of partial shapes freely [4,7-12]. In this regard, laser powder bed fusion (LPBF) technology, a type of metal AMs, is a method of stacking the material layer by layer on a powder bed by irradiating laser and has the highest precision among the metal AMs. [4,9-13].Several attempts have been made to overcome the limitations of low mechanical properties due to nodes of the existing strut-based lattice [14,15]. To this end, high-performance, multi-purpose materials were employed via synthesis of lattices of unique shape using the LPBF process. [10,16,17].

Ideal lattices that comprise a triply periodic minimal surface (TPMS) as unit cell have recently attracted attention. TPMS is defined as a 3D surface shape consisting of a minimal surface [14,16,18-21]. Since TPMS has no node and consists of smooth sheets, it has even stress distribution under an applied load, giving rise to excellent mechanical properties. Moreover, since two independent spaces have an open pore structure, TPMS exhibits a significantly higher specific surface area than conventional lattices [14,16,18-21]. I-wrapped package (I-WP), a leading TPMS model, was derived from the structure of BCC strut-based lattice and is known to exhibit excellent rigidity and high energy absorption characteristics among the TPMS models [14,20,21].

Co-Cr-Mo alloy is used in medical parts such as dental implants and hip joint sockets and balls due to its excellent biocompatibility and wear performance. [22-25]. It has been reported that strut-based lattices applied a Co-Cr-Mo alloy have longer fatigue life and more excellent energy absorption efficiency than other biomaterials [26]. This is expected to be related to the microstructural deformation behavior of Co-Cr-Mo alloys, but studies related to this are very insufficient. In addition, when the Co-Cr-Mo alloy is applied to the TPMS model, it is expected to exhibit better physical properties.

In the current study, sheet I-WP lattices were formed via LPBF process using Co-Cr-Mo alloy, and the structure and compression characteristics of the lattices were investigated.

[1] INHA UNIVERSITY, DEPARTMENT OF MATERIALS SCIENCE AND ENGINEERING, INCHEON, KOREA
[2] AGENCY FOR DEFENSE DEVELOPMENT, DAEJEON, KOREA
[3] INTERDISCIPLINARY RESEARCH CENTER FOR INTELLIGENT MANUFACTURING & ROBOTICS, KING FAHD UNIVERSITY OF PETROLEUM & MINERALS, DHAHRAN, SAUDI ARABI

* Corresponding author: keeahn@inha.ac.kr

The findings were further compared with the characteristics of LPBF-built bulk Co-Cr-Mo alloy to identify the deformation behavior of the sheet I-WP lattice.

2. Experimental

Sheet-type I-WP model [14,19] was used as unit cell of size $1\times1\times1$ mm^3. The lattice structure was composed of 5×5×5 unit cells. To form thin sheets, no specification on the thickness of the sheet was provided by the design but let the sheet be formed along the path of irradiation of the laser in the LPBF process.

Spherical Co-29Cr-6Mo alloy powder feedstock (MTT Technologies, Germany) was produced via gas atomization and 30 μm or less sized particles were collected through sieving. In the LPBF process, MCP HEK REALIZER (SLM Solutions GmbH, Germany) equipment was used to prepare specimens under the following conditions-layer thickness: 30.0 μm, exposure time: 0.17 ms, point distance: 640 μm, laser power: 90 W, and scanning rate: 376 mm/s. And the scanning route of each layer was specified to rotate clockwise along the lines defined by the sheet cross-section.

Micro-computed tomography (μ-CT, Skyscan, Aartselaar, Belgium) was also performed under the condition of 100 kV, 100 μA, and 700 ms, and voxel size of 17.6 μm, and reconfigured it to a 3D model using the CTvox software (BRUKER). FE-SEM (TESCAN, MYRA3 XMH) study was performed to observe the cross-sectional shape of the specimens before and after deformation. The specimens were polished with 1200-4000 grit silicon carbide papers and mirror-finished with a diamond suspension of 1 μm diamond and 0.04 μm colloidal silica. Afterward, EBSD analysis was done using an electron backscatter diffraction detector (EBSD, OXFORD, Symmetry) fitted to the FE-SEM. The EBSD data were processed with OIM analysis software (TSL OIM analysis 8).

A room-temperature compression test was conducted at initial strain rate of 1×10^{-3} s^{-1} using the Instron 8501 equipment (Instron, USA). Compression was performed perpendicularly to the building direction. To compare the mechanical properties with the bulk alloy, bulk Co-Cr-Mo was manufactured through the LPBF process under the same conditions with lattice, processed to pellets having 3 mm in diameter and 6 mm in height. A compression test was conducted under the same conditions. When comparing the mechanical properties of bulk and lattice materials, a load was commonly applied perpendicular to BD to minimize the effect of high anisotropy in LPBF-built metals [23].

3. Results and discussion

Fig. 1 (a) shows the computer-aided design applied to the lattice manufacturing, and Fig. 1(b) displays the micro-CT image of the lattice manufactured by the LPBF process. The orientation of the specimen was divided into the building direction (BD), the longitudinal direction (LD and compressive direction), and normal direction (ND) perpendicular to the BD and LD. The produced lattice exhibited the pore shape of the I-WP model well and was confirmed to have a smooth surface. The relative density (RD), as calculated from the lattice's weight and volume and the true density of the Co-Cr-Mo alloy was 59.3%.

The SEM image of the cross-section of the sheet I-WP lattice (Fig. 2(a)) was examined, and EBSD analysis of its initial microstructure was performed. The results from three representative areas are shown in Fig. 2 (b), (c) and (d). Cross-sectional observation of the lattice revealed that the sheet thickness was about 170 μm. Analysis of the phase map showed that the measured fractions of the hexagonal closed packed (HCP) phase and face-centered cubic (FCC) phase was 4.9% on average and 95.0% or more, respectively. For the Co-Cr-Mo alloy, the HCP phase is known to be stable at 900°C or below [22]. However, the FCC phase was dominant in the specimen made in the present study, which can be attributed to the high cooling rate of the SLM process resulting in the metastable FCC phase even at room temperature [22,23]. Analysis of the inverse pole figure (IPF) map showed that the grains have a wide range of size distribution and the grains in the outer region of the sheet were relatively finer. Analysis of the kernel average misorientation (KAM) map and boundary angles revealed the presence of local strains and low angle boundaries inside the grains which were due to fast-cooling rate of the LPBF process. These low angle boundaries and initial dislocations are believed to have helped improve the strength of the lattice and bulk alloy [27].

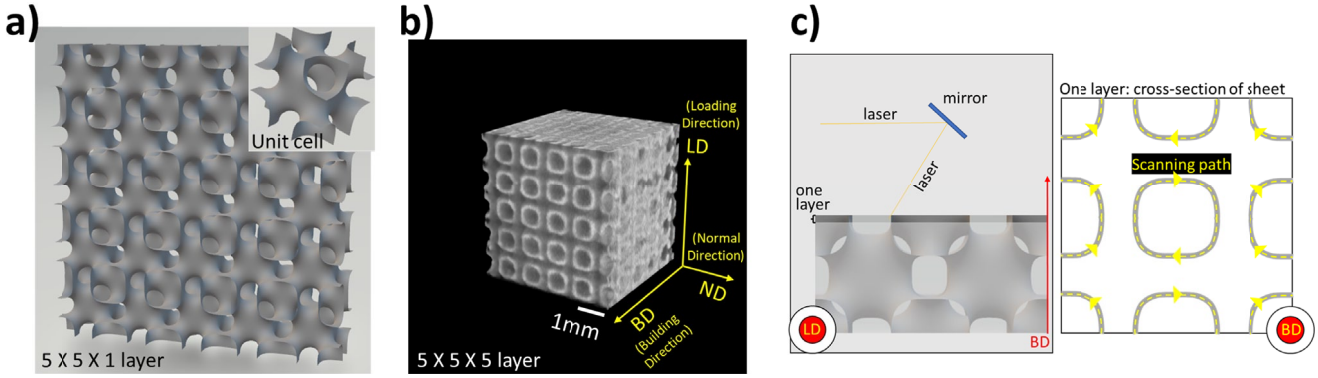

Fig. 1. Images of I-WP model: (a) computer aided design of unit cell and cell layer, (b) micro-CT analysis result of additively manufactured lattice with cartesian coordination, and (c) the schematic diagram showing strategy of LPBF process

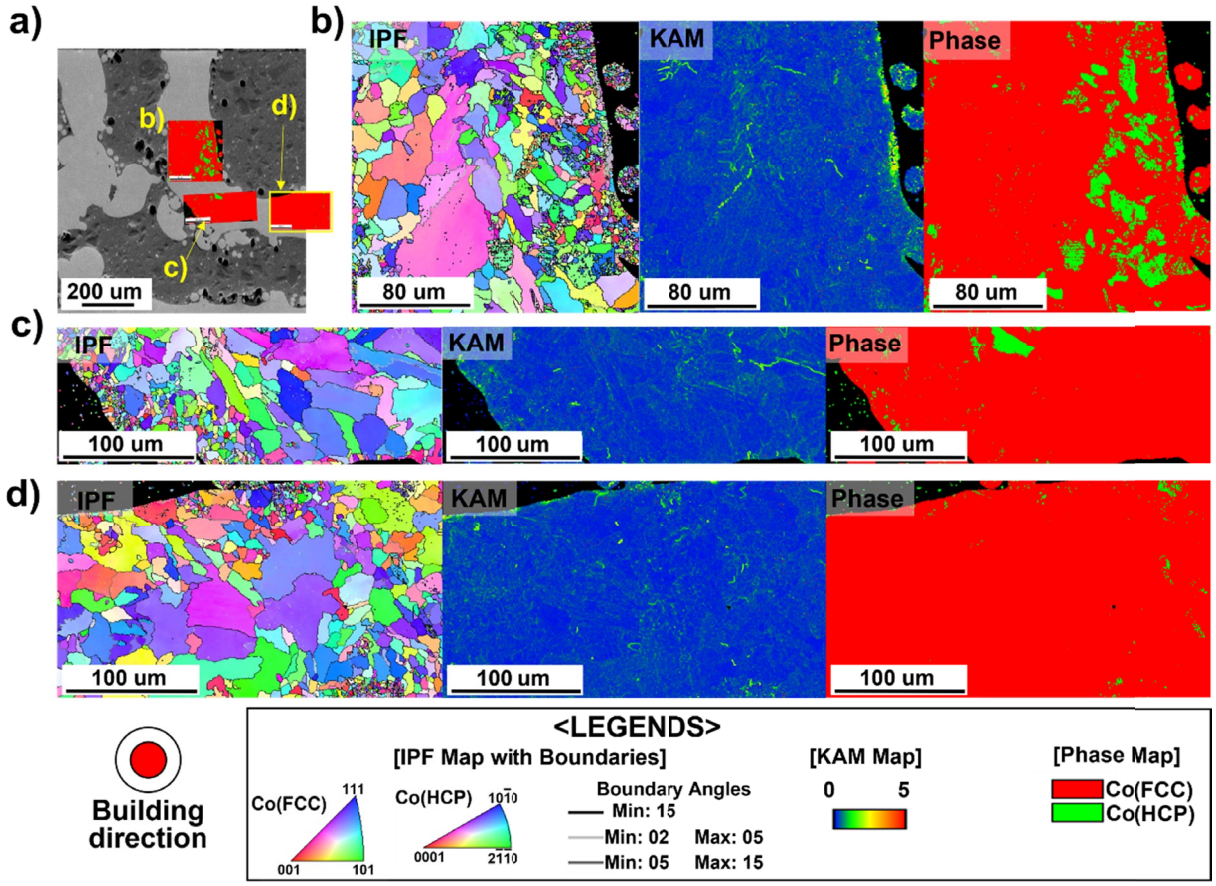

Fig. 2. (a) Cross-sectional SEM micrograph of initial I-WP lattice, and (b), (c), (d) the EBSD analysis results (IPF, KAM and Phase map) of representative areas

Fig. 3 shows compression test results of the bulk Co-Cr-Mo and sheet I-WP lattice along with the compressive deformed (about 40%) lattice (inset image of Fig. 3(b)). The macroscopic observation of the deformed shape of the sheet I-WP lattice showed the formation of double shear bands in "X" shape. Although the degree of deformation varied with location, horizontal deformation bands were formed similarly on each cell layer and showed a tendency of collective failures. The stress-strain curve of bulk Co-Cr-Mo showed a linear increase in flow stress after yielding, followed by fracturing after reaching a strain of about 23.7% and a strength of 1.6 GPa. Due to the relatively high RD of lattice, the stress-strain curve of sheet I-WP lattices was Similar to that of the bulk specimens, which showed near-linearly increased flow stress after yielding and then gradual fracturing after reaching a strain of about 42.6% and a strength of 630.1 MPa. The yield strengths of the bulk and lattice were found as 810.4 MPa and 176.3 MPa, respectively. According to Gibson and Ashby et al. [28], the relationship

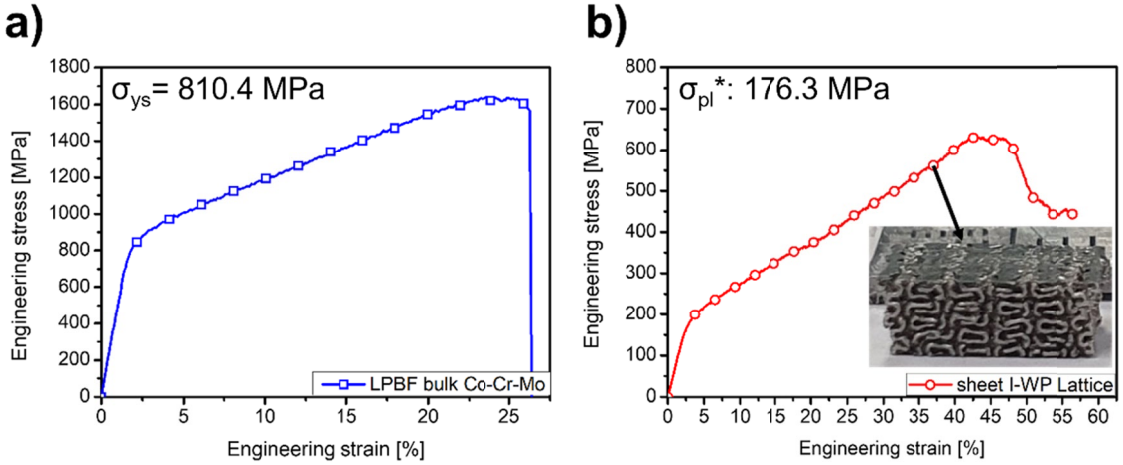

Fig. 3. Results of compressive test; (a) strain-stress curve of LPBF bulk Co-Cr-Mo alloy, (b) that of sheet I-WP lattice with compressively deformed (about 40%) lattice (inset image)

between the relative density and yield strength of an open lattice with relative density of 30% or more can be expressed by Equation (1), which is known as modified Gibson-Ashby model. Therefore, the yield strength can be obtained according to the density from this equation.

$$\frac{\sigma_{pl}^{*}}{\sigma_{ys}} \approx 0.23\left(\frac{\rho^{*}}{\rho_{s}}\right)^{1.5}\left[1+\left(\frac{\rho^{*}}{\rho_{s}}\right)^{0.5}\right] \quad (1)$$

Here, σ_{pl}^{*} refers to the plastic yield strength of the lattice, and σ_{ys} refers to the yield strength of the bulk alloy. ρ^{*}/ρ_{s} refers to the RD of the lattice. When RD was 59.3%, the estimated σ_{pl}^{*} was 150.7 MPa, indicating that the yield strength of the actual lattice was 25.6 MPa higher. This signified that the strength of the manufactured sheet I-WP lattice was higher than the relative density and can be considered to be related to the geometrical characteristics of I-WP or the deformation behavior of the applied alloy.

Fig. 4 shows the cross-sectional SEM image of the deformed sheet I-WP lattice and EBSD analysis results of the I-WP deformation behavior. Observation of the KAM map showed that deformation occurred in various locations of the lattice. From the phase map study, the HCP phase fraction according to location was measured as (b) 34.1% (c) 47.7% (d) 20.3%, which shows a significant increase in the HCP fraction compared to the initial fraction. This is related to the Co-Cr-Mo alloy's strain-induced martensitic transformation (SIMT) deformation behavior [22-25] caused by stacking fault energy of 15 mJ/m^2 or lower. Such SIMT behavior resulted in a high strain-hardening effect while accommodating strains through transformation of inside grains, and thus, enabled the Co-Cr-Mo alloy to have an excellent strength-ductility combination [22-26]. The excellent strength-ductility combination and high strain-hardening rate of the alloy applied to lattices not only delayed fracture due to local strain but also accommodated the load evenly inside the grains, leading to additional load energy absorption and improved mechanical properties. In particular, since sheet I-WP had a collective deformation mode that accommodated even deformation throughout the structure, SIMT generation was expected to be higher. In other words, LPBF Co-Cr-Mo sheet I-WP lattices were determined to show excellent mechanical properties compared to the relative density due to uniform deformation of the I-WP shape and the synergetic effect of the SIMT behavior of the Co-Cr-Mo alloy.

4. Conclusions

This study manufactured sheet I-WP lattices applying Co-Cr-Mo alloy in the SLM process, investigated its mechanical properties, and analyzed them in connection with the geometrical features of the unit cell. Calculation of the yield strength com-

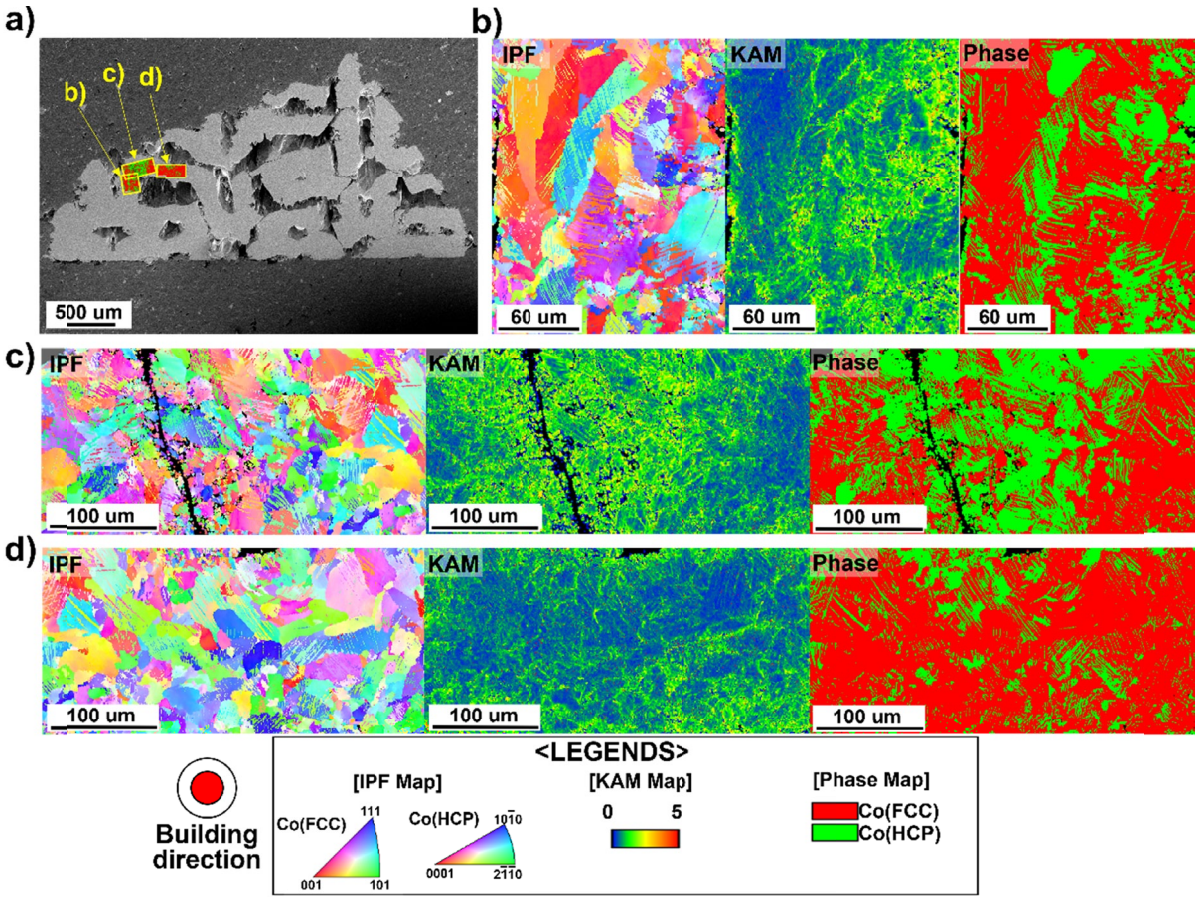

Fig. 4. (a) Cross-sectional SEM image of deformed I-WP lattice, and (b), (c), (d) the EBSD analysis results (IPF, KAM and Phase map) of representative areas considering I-WP's deformation behavior

pared to the relative density by applying the modified Gibson-Ashby model confirmed that the lattices exhibited excellent specific strength. The results of the deformation behavior of the sheet I-WP lattice showed that the deformation was uniformly distributed throughout the structure. Microstructural study after deformation showed that the load was accommodated by generating a high SIMT fraction. As a result, it was suggested that the LPBF Co-Cr-Mo based sheet I-WP lattice has excellent specific strength.

Acknowledgments

This research was supported by Korea Institute for Advancement of Technology (KIAT) grant funded by the Korea Government (MOTIE) (P0002007, The Competency Development Program for Industrial Specialist)

REFERENCES

[1] C. Pan, Y. Han, J. Lu, Appl. Sci. **10** (18), 6374 (2020).
[2] L.J. Gibson, Mater. Sci. Eng. **A 110**, 1-36 (1989).
[3] A.G. Evans, J.W. Hutchinson, M.F. Ashby, Prog. Mater. Sci. **43**, 171-221 (1999).
[4] T. Maconachie, M. Leary, B. Lozanovski, X. Zhang, M. Qian, O. Farugue, M. Brandt, Mater. Des. **183**, 108137 (2019).
[5] V.S. Deshpande, N.A. Fleck, M.F. Ashby, J. Mech. Phys. Solids **49**, 1747-1769 (2001).
[6] J. Zhou, P. Shrotriya, W.O. Soboyejo, Mech. Mater. **36**, 723-737 (2004).
[7] C. Yan, L. Hao, A. Hussein, S.L. Bubb, P. Young, D. Raymont, J. Mater. Process. Technol. **214**, 856-864 (2014).
[8] P. Heinl, L. Müller, C. Körner, R.F. Singer, F.A. Müller, Acta Biomater. **4**, 1536-1544 (2008).
[9] S. McKown, Y. Shen, W.K. Brookes, C.J. Sutcliffe, W.J. Cantwell, G.S. Langdon, G.N. Nurick, M.D. Theobald, Int. J. Impact Eng. **35**, 795-810 (2008).
[10] C. Yan, L. Hao, A. Hussein, D. Raymont, Int. J. Mach. Tool Manufact. **62**, 32-38 (2012).
[11] L. Mullen, R.C. Stamp, W.K. Brooks, E. Jones, C.J. Sutcliffe, J. Biomed. Mater. Res. B Appl. Biomater. **89B** (2), 325-334 (2009).
[12] O. Rehme, C. Emmelmann, J. Laser Micro Nanoeng. **4** (2), 128-134 (2009).
[13] E. Louvis, P.Fox, C.J. Sutcliffe, J. Mater. Process. Technol. **211**, 275-284 (2011).
[14] C. Yan, L. Hao, A. Hussein, D. Raymont, Mater. Des. Process. Commun. **e205**, 3 (2021).
[15] A. Zargarian, M. Esfahanian, J. Kadkhodapour, S. Ziaei-Rad, Mater. Sci. Eng. C **60**, 339-347 (2016).
[16] L. Yang, R. Mertens, M. Ferrucci, C. Yan, Y. Shi, S. Yang, Mater. Des. **162**, 394-404 (2019).
[17] C. Yan, L. Hao, A. Hussein, P. Young, D. Raymont, Mater. Des. **55**, 533-541 (2014).
[18] I. Maskery, N.T. Aboulkhair, A.O. Aremu, C.J. Tuck, I.A. Ashcroft, Addit. Manuf. **16**, 24-29 (2017).
[19] S.-Y. Park, K.-S. Kim, B. AlMangour, D. Grzesiak, K.-A. Lee, Mater. Des. **206**, 109778 (2021).
[20] O. Al-Ketan, R.K.A. Al-Rub, J. Mater. Res. **33** (3), 343-359 (2018).
[21] A.S. Dalaq, D.W. Abueidda, R.K.A. Al-Rub, Compos. Part A-Appl. S. **84**, 266-280 (2016).
[22] A. Takaichi, Suyalatu, T. Nakamoto, N. Joko, N. Nomura, Y. Tsutsumi, S. Migita, H. Doi, S. Kurosu, A. Chiba, N. Wakabayashi, Y. Igarashi, T. Hanawa, J. Mech. Behav. Biomed. **21**, 67-76 (2013).
[23] K.-S. Kim, J.-W. Hwang, J. Alloys Compd. **834**, 155055 (2020).
[24] A. Chiba, K. Kumagai, N. Nomura, S. Miyakawa, Acta Mater. **55**, 1309-1318 (2007).
[25] M. Mori, K. Yamanaka, A. Chiba, J. Mech. Behav. Biomed. Mater. **55**, 201-214 (2016).
[26] S.M. Ahmadi, R. Hedayati, Y. Li, K. Lietaert, N. Tümer, A. Fatemi, C.D. Rans, B. Pouran, H. Weinans, A.A. Zadpoor, Acta Biomater. **65**, 292-304 (2018).
[27] C. Bonatti, D. Mohr, J. Mech. Phys. Solids **122**, 1-26 (2019).
[28] L.J. Gibson, M.F. Ashby, Cellular solid: structure and properties, 2nd ed., Cambridge University, Cambridge (1997).